Eurographics Workshop on Visual Computing for Biology and Medicine (2015)
K. Bühler, L. Linsen, and N. W. John (Editors)

Schematic Electrode Map for Navigation in Neuro Data Sets

C. Schulte zu Berge[1], J. Weiss[1], and N. Navab[1,2]

[1]Computer Aided Medical Procedures, Technische Universität München, Germany
[2]Computer Aided Medical Procedures, Johns Hopkins University, USA

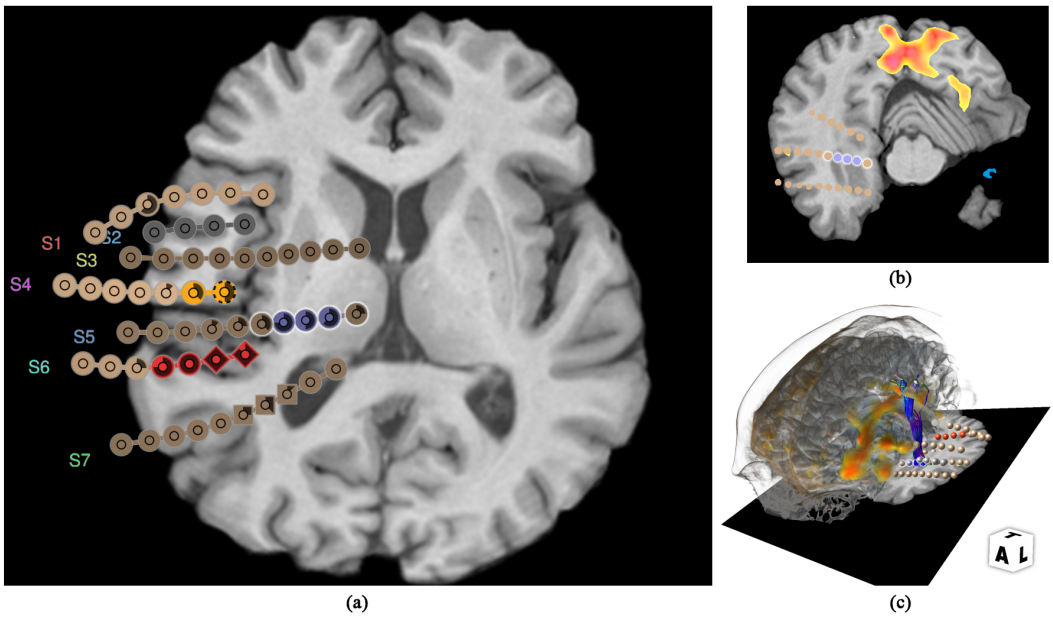

Figure 1: (a) Our proposed **schematic electrode map with the electrode glyph** showing an overview over the depth electrode configuration. Furthermore, it serves as a navigation tool for linked multi-modal visualizations, e.g. (b) definition of the 2D MPR plane; (b) camera placement or DTI fiber filtering in 3D volume rendering.

Abstract

Neuro resection surgery is one of the last resorts when treating epilepsy patients where conservative treatment shows no effect on seizure reduction. However, due to the severity of the surgery, the resection planning has to be as precise as possible in order to avoid harming any critical anatomy. The tight time constraints in clinal routine demand for a highly optimized workflow. In this work, we therefore introduce a novel visualization in order to simplify the navigation in the complex multi-modal neuro data sets and support the clinician with the planning procedure. We propose a schematic electrode map based on a force-directed graph model providing an intuitive overview over the topology of the implanted depth electrode configuration. To further facilitate the planning workflow, our carefully designed electrode glyph supports different scalar, nominal and binary annotations augmenting the view with additional information. Brushing and linking techniques allow for easy mapping of the EEG data to the corresponding anatomy, as well as for straight-forward navigation within the visualization of the anatomical and functional imaging modalities in order to identify the origin and spread of the seizure. Our results show that the proposed graph layouting method successfully removes occlusions of the projected electrodes while maintaining the original topology of the depth electrode configuration. Initial discussions with clinicians and the application to clinical data further show the effectiveness of our methods.

Categories and Subject Descriptors (according to ACM CCS): I.3.m [Computer Graphics]: Miscellaneous— J.3 [Computer Applications]: Life and Medical Sciences—Health

DOI: 10.2312/vcbm.20151223

1. Introduction

Epilepsy describes a neurological disorder that is characterized by recurring seizures, which usually manifest as episodes of involuntary movement of the body. In cases where conservative treatment shows no effect on seizure reduction, resection of the seizure-inducing brain matter may be indicated [BG15]. These seizures are the result of synchronized excessive electrical discharges often focused to a certain region of the brain. Since identifying this part of the brain is a prerequisite for the surgery, the implantation of depth electrodes and the analysis of their EEG data [PJ54] is one of the most important tools for resection surgery planning. By using the implanted electrodes for electrical stimulation under local anesthesia, it is possible to map areas where sensory, language or visual function is impaired [KF03, Sil12]. However, this insight needs to be closely correlated with possible findings in both anatomical and functional imaging of the corresponding anatomy. Since neuro surgery exposes a minimal margin for error, the planning clinician has to make sure to not only identify the correct origin of the seizure but also to identify critical brain regions such as the language center or the visual center that must not be harmed at all cost.

While epilepsy surgery planning is a highly specialized task, clinical routine often poses tight time constrains to the clinician for the actual planning performance. The analysis of the many different modalities and in particular the mapping of the EEG data to the spatial images of the brain imposes a high cognitive load to the clinician and requires a lot of interaction with the planning software. Our work was developed to specifically support such planning workflow. We propose a glyph-based schematic view showing the electrode configuration with respect to the MRI anatomy. By employing force-directed graph layouting methods, we are able to generate a schematic map of arbitrary projection which provides the user with an intuitive overview. To depict relative glyph positions together with multiple per-electrode annotations, we designed an electrode glyph supporting scalar, nominal and binary annotations. By integrating various brushing and linking techniques, our visualization can then be used as an easy navigation tool for the underlying multi-modal data. This allows the clinician to inspect the target electrode's surrounding anatomy in additional views in order to correlate the EEG data with the anatomical and functional images.

1.1. Clinical Application and Workflow

While we expect our proposed schematic view to be useful in any clinical tasks that include depth electrodes, we designed our methods to suit the particular workflow of brain resection planning for epilepsy patients based on depth electrode EEG (cf. Figure 2). In collaboration with our clinical partner, we analyzed the typical workflow during a planning session and identified five different stages:

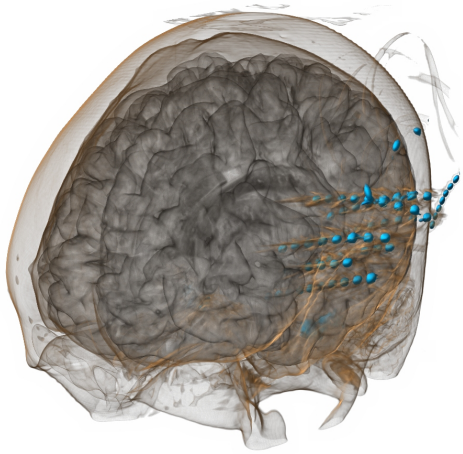

Figure 2: Direct Volume Rendering of a co-registered CT-MRI **reference data set illustrating the electrode configuration** with respect to the anatomy. The cyan spheres represent the contacts of the depth electrodes implanted into the left hemisphere of the patient's brain.

1. **Data Set Co-registration.** The clinician gathers the available data sets and co-registers them to fit to a common coordinate system.
2. **Electrode Segmentation.** The clinician segments the depth electrodes from the CT data set and creates corresponding geometry for rendering.
3. **EEG Analysis.** The clinician analyzes the EEG data to identify the electrodes corresponding to the seizure origin as well as to assess the progression of the seizure.
4. **Multi-modal Data Analysis.** The clinican maps the electrodes' EEG information to the multi-modal data set and studies the surrounding anatomy as well as the available functional data. Thereby, he identifies the corresponding brain regions and further assesses pathological findings as well as any functional abnormalities.
5. **Development of a Resection Proposition.** The clinician creates a map for the operating surgeon defining which specific region should be resected. Furthermore, he annotates the electrodes in the map with different labels indicating the relative number of electrical discharges or organs at risk (e.g. language center, optical center).

Our work was designed to support the clinicians with this particular workflow. However, we do not target steps 1 and 3, since both multi-modal co-registration and EEG analysis are outside the scope of this work. We can safely assume the multi-modal registration problem to be sufficiently solved [PB13]. Furthermore, our clinical partner asserted that the available tools for EEG analysis are already highly specialized and therefore hard to integrate with the rest.

1.2. Related Work

Since this clinical workflow covers a lot of different topics, the corresponding body of literature is large. Therefore, we focus this section on the most closely related works regarding our particular methods and refer the interested reader to the book of Preim and Botha [PB13] for a more exhaustive overview.

In terms of medical image segmentation, a large variety of methods exist, often specialized for particular applications. Regarding depth electrode segmentation, two recent papers are of particular interest: Taimouri et al. developed a system to automatically localize electrodes in a pediatric head CT acquired for resection planning of the seizure onset zone [TAATF*14]. By combining thresholding with morphologic filtering, they are able to segment the electrodes from a CT scan and project them onto a smoothed cortical surface for visualization using the gyri and sulci as orientation cues. Arnulfo et al. describe a fast, accurate automatic segmentation algorithm relying on the planned positions of target and entry points [ANC*15].

For neuro surgery planning with its minimal margin for error, multi-modal visualization techniques are required in order to show both functional and anatomical information in the same reference frame. Beyer et al. present an elaborate system for pre-operative planning of neurosurgical interventions, which is capable of real-time volume rendering several data sets including focus-and-context visualization using their proposed GPU skull peeling algorithm [BHWB07]. The work of Rieder et al. also focuses on neuro surgery planning and additionally supports the visualization of DTI fiber tracts [RRRP08]. In their work they propose and discuss different glyphs to support the observer with localization cues for deep objects in 3D renderings. Diepenbrock et al. present another integrated visualization platform for neuro surgery planning, which offers intuitive interaction metaphors to interactively define and assess access paths in linked multi-modal 2D and 3D views [DPL*11]. Targeting the specialized workflow of Deep Brain Stimulation (DBS), Bock et al. propose a set of different visualizations supporting the clinician during the entire DBS workflow of (pre-operative) planning, recording (intra-operative imaging) and (electrode) placement while paying special attention to the uncertainty present in the different modalities [BLE*13].

For the creation of our proposed schematic view, we model the depth electrode configuration as an undirected graph, which we embed into a 2D projection. For general graph layouting, a large variety of algorithms exist for different types of graphs and different applications [DB99,Sug02]. For our specific application, we selected a force-directed layouting approach, where the graph is modeled as a set of springs exerting forces on the positions of the nodes. As originally proposed by Fruchterman and Reingold, an optimal graph layout is defined by the minimal energy configuration of such a force field [FR91].

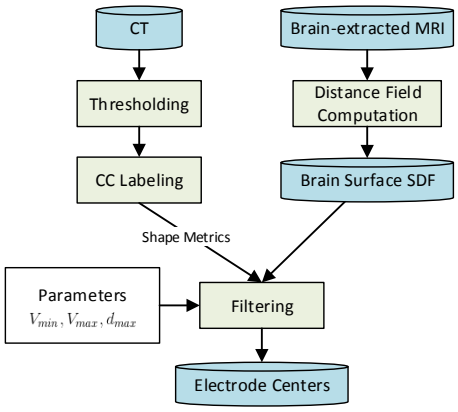

Figure 3: Illustration of the **segmentation pipeline** to compute the centroid position of each electrode.

2. Methods

Within this work, we present a novel visualization tool, which facilitates the navigation within multi-modal neuro data sets, consisting of the following main contributions:

- A schematic 2D view of the segmented depth electrodes maintaining the original topology based on a force-directed graph formulation.
- A glyph design supporting different scalar, nominal and binary annotations used to represent electrodes during rendering of the schematic view.
- A set of brushing and linking concepts in order to use the schematic view as a navigation tool for the underlying multi-modal data.

For our methods we assume to have at least one CT volume showing the implanted depth electrodes, as well as one T_1-weighted brain-extracted [SDB*04, BRS*04] MRI volume showing the brain's soft tissue, available (cf. Figure 2). However, any other anatomical or functional imaging modality can be easily integrated with the system in order provide more information to the clinician. For demonstration, we show the integration of both PET and DTI data into our proposed system.

2.1. Electrode Segmentation from CT

In an initial preprocessing step, we segment the electrode contacts from the CT volume in order to capture the topology of the implanted depth electrodes. After discussions with our clinical partner, we decided to perform this segmentation in a semi-automatic fashion, as this is sufficient for our particular workflow. More advanced techniques, such as [TAATF*14, ANC*15], may thus yield better results. Figure 3 illustrates our segmentation pipeline.

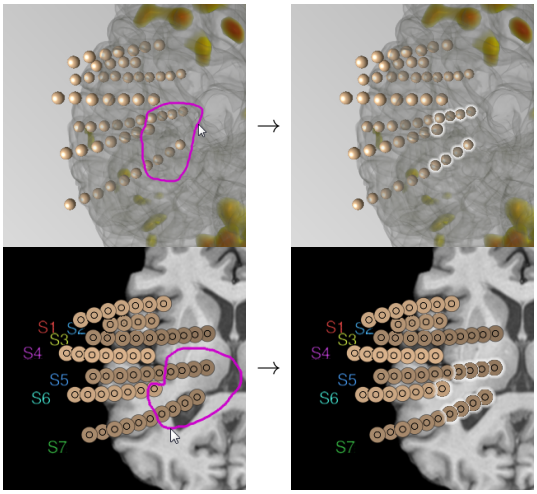

Figure 4: Illustration of the **lasso selection metaphor**, which can be applied to any view showing the electrodes. By drawing a freehand polygon into the projection (*left column*), the user can select a group of electrodes. The selection state is visualized through a glow effect (*right column*).

In a first step we identify the single electrode contacts through thresholding at 2000 HU followed by a connected component analysis. Since the resulting segmentation includes noise, artifacts, as well as regions outside the brain, we annotate each segmented region with its centroid, volume bounding box, and roundness metric. In a subsequent filtering process we use these shape metrics to identify possible electrodes.

- Since the physical dimensions of the electrodes are known, we can filter the segmented regions by shape and size.
- To remove segmented regions outside of the brain, we check each region's centroid against a signed distance field of the brain surface computed from the brain-extracted T_1 volume.

In a final step, we semi-automatically identify the topology of the depth electrodes. The segmented electrode contacts are displayed in the standard 2D MPR and 3D volume rendering visualizations of the volumes. The user then marks all contacts belonging to a single depth electrode through a lasso selection (cf. Figure 4 and Section 2.4.1) in one of the available views. Since the camera of the views is freely adjustable, one can easily find projections where the depth electrodes separate well. The electrode definition can be fine-tuned through an additional single selection metaphor. Once a group of contacts is defined as a depth electrode, we order the contacts sequentially with respect to their depth. To determine the order, we identify the contact with minimum penetration depth (i.e. the contact being the most outside the brain according to the signed distance field) and then sort the remaining contacts by their distance to this contact, defining the furthest one as tip of the depth electrode. In cases where the depth electrode is inserted very deep into the brain, this method has proven to be more robust than sorting the contacts directly based on the signed distance field.

2.2. Schematic Electrode View

During neuro resection planning the clinician has to map the information gained from EEG to the brain anatomy shown in the MRI in order to identify the region where the seizure originates from. Further imaging modalities such as PET or DTI may provide him with additional insight on functional abnormalities or other pathological findings, which refines his idea on which brain regions are the source of the seizures and which regions must not be resected at all cost. When handling such large amount of information, clinicians are required to build a complex mental model of the findings.

In order to support their workflow and provide the user with an intuitive navigation tool for the high-dimensional multi-modal data, we propose a schematic view of the depth electrode configuration in their anatomical context, which was designed with the following goals:

- **Occlusion free.** When projecting the 3D electrode configuration to a schematic 2D view, some of the electrodes may occlude each other. However, since our visualization is intended as a navigation tool, such occlusion needs to be prevented at all cost because each electrode should be directly pickable.
- **Topology preserving.** While the schematic view should show some kind of abstraction of the electrode configuration, it should preserve its topology, since the relative positioning of the electrodes to each other is an important localization cue for reference.
- **Intuitiveness.** The expert should be able to quickly understand the view and intuitively map the relations between it and other data views (e.g. 2D MPR, 3D volume rendering).
- **Accuracy.** Since the schematic view shows the electrode configuration with respect to the surrounding anatomy, the spatial relations should be depicted as accurately as possible.

2.2.1. Graph Layouting

In order to satisfy these goals, we model the electrode configuration as a graph, which is then layouted using a force-directed approach. The graph $G = (V, E)$ is defined as a set of vertices $v \in V$ corresponding to the electrode centers and a set of edges $e \in E = V \times V$ between the vertices. For our problem, we model two vertices as being connected if they belong to the same depth electrode and are adjacent to each other. Hence, in the non-degenerate case, every vertex has either one or two adjacent edges and the graph is composed of several disconnected subgraphs corresponding to the implanted the depth electrodes.

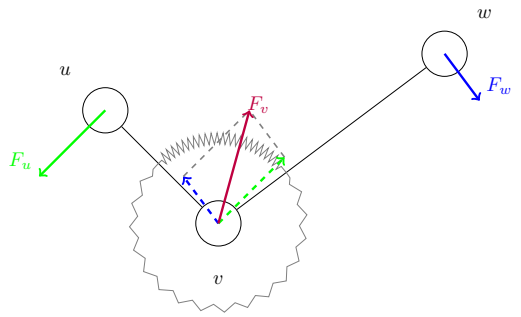

Figure 5: Illustration of the **angular forces** exerted on the three vertices by the two radial springs inserted between the edges at vertex v. The upper spring pushes the edges apart while the lower one pulls them together.

In order to embed G in arbitrary 2D projections according to the above criteria, we employ a force-directed approach inspired by Fruchterman and Reingold [FR91]. We model the graph as a mass-spring system, which is striving to minimize its inherent energy configuration. Each vertex $v \in V$ is modeled as a mass-less point at position p_v, with its initial position p_v^* defined as the 2D projection of the 3D electrode position. Furthermore, the vertices are modeled as electrical charges of the same polarity, thus exerting repulsion forces on each other governed by Coulomb's law

$$F_C(u,v) = C \cdot \frac{q_v \cdot q_u}{|p_v - p_u|^2} \frac{p_v - p_u}{|p_v - p_u|}, \tag{1}$$

where C is a scaling constant and q_u, q_v are the electric charges of the respective vertices. For simplicity, we model the charges to be 1 for all vertices. Each edge between two vertices u, v is modeled as a spring governed by Hooke's law

$$F_H(u,v) = H \cdot \left(|p_v - p_u| - L\right) \frac{p_v - p_u}{|p_v - p_u|}, \tag{2}$$

where L is the initial spring length (i.e. $|p_v^* - p_u^*|$) and H the spring stiffness constant.

The repulsion forces (Eq. 1) will push the subgraphs apart indefinitely, since they are not connected with each other. Therfore, we introduce an additional *homing force*, which pulls each vertex v towards its original position p_v^*

$$F_O(v) = O \cdot \left(p_v^* - p_v\right), \tag{3}$$

where O is the homing force scaling constant.

Finally, we introduce an *angular force* that pushes to equalize angles between the edges of a vertex. This force serves as straightening of the graph lines of each depth electrode, which is highly desirable. Without this force, the combination of repulsion force (Equation 1) and homing force (Equation 3) may yield jagged lines in cases where the vertices are too close to each other. We model the angular force as additional radial springs, which are jammed between each pair of adjacent edges and pushing apart edges whose angle is too small and pulling together edges whose angle is too large. For the angle between three adjacent vertices u, v, w this yields three forces F_v, F_u and F_w as illustrated in Figure 5. Given α as the angle between $(u,v),(v,w) \in E$, we compute the torque as the difference between α and the optimal angle multiplied with a scaling factor A

$$\tau = A \cdot \left(\alpha - \frac{2\pi}{\deg(v)}\right). \tag{4}$$

The torque defines the rotation forces of u, w around v

$$\begin{aligned} F_u(u,v) &= \frac{\tau}{|p_u - p_v|} \begin{pmatrix} -\hat{d}_{u,y} \\ \hat{d}_{u,x} \end{pmatrix}, \\ F_w(v,w) &= -\frac{\tau}{|p_w - p_v|} \begin{pmatrix} -\hat{d}_{w,y} \\ \hat{d}_{w,x} \end{pmatrix} \end{aligned} \tag{5}$$

where $\hat{d}_u$ and $\hat{d}_w$ are the normalized direction vectors from v towards u and w, respectively. Furthermore, vertex v is pulled towards the center of u and w by the negative of the two radial forces

$$F_A(u,v,w) = F_v(u,v,w) = -\left(F_u(u,v) + F_w(v,w)\right). \tag{6}$$

These forces are computed for each angle between two adjacent edges.

An optimally layouted graph is defined, such that the total energy configuration of our model is minimal. Thus, our method minimizes the energy term

$$E_{\text{tot}} = \sum_{v \in V} \|F(v)\|, \tag{7}$$

where the per-vertex force is defined as

$$\begin{aligned} F(v) = &\sum_{\substack{u \in V \\ u \neq v}} F_C(u,v) + \sum_{(u,v) \in E} F_H(u,v) \\ &+ F_O(v) + \sum_{\substack{u,w \in V \\ (u,v) \in E, (v,w) \in E}} F_A(u,v,w). \end{aligned} \tag{8}$$

Since this is a high-dimensional non-linear problem, a direct minimization is not feasible for real-time applications. Instead, we find a local minimum by iteratively moving the vertices in the direction of the net force exerted on each vertex. To improve the convergence behavior, we introduce a damping factor η, which distributes the forces over several iterations.

2.3. Visualization

For our schematic view of the electrode configuration we perform an illustrative rendering of the layouted graph. We render the vertices representing single electrodes using point sprite glyphs and further render line primitives for the edges representing the grouping into depth electrodes.

2.3.1. Electrode Glyph

To represent a single electrode contact, we designed the basic electrode glyph to have a circular shape containing a smaller black circle outline in the center to mimic the appearance of a real-world electrode contact. Furthermore, we define a number of glyph parameters that can be used to map different scalar, nominal and binary attributes. As discussed in the previous sections, the clinician performs an extensive assessment of the findings in the different modalities and compiles a resection map for the surgeon. Our electrode glyph allows to map these findings to the different glyph parameters and thereby annotate the schematic view with clinically relevant information. Since the visual variables of spatial position and size are already fixed in our visualization we map those annotations to the following parameters:

- **Glyph color.** The glyph background color can be used for nominal annotations, for instance to depict certain functional regions of the brain.
- **Glyph shape.** The glyph shape can be used to nominally annotate other abnormalities. In order to keep the glyphs easily distinguishable from each other, we restrict the number of shapes to circle, quadrangle and diamond.
- **Glyph filling.** In order to support scalar or ordinal annotations, we integrate a clock glyph into our electrode glyph, which visualizes the quantity by filling the glyph clockwise with an opaque color. The values are mapped from zero rendered as a completely empty circle to the maximum rendered with a completely filled circle.
- **Glyph border.** Finally, to support important binary annotations, we allow a stipple border for the electrode glyph. Since this is a rather powerful visual cue, it should be used with care.

Figure 6 shows our proposed electrode glyph in its different configurations.

2.3.2. Anatomical Context

For an additional spatial reference of the electrodes with respect to the anatomy, we augment the rendered graph with a slice of matching orthographic projection of the MRI volume. We select the slice such that it runs through the center of the volume and its orientation is always perpendicular to the viewing direction. This way, our visualization provides the observer with good spatial cues for the orientation and position of the electrodes. The final visualization is illustrated in Figure 1 (a).

In order to improve the depth perception of the electrodes with respect to the current projection, we add an additional depth cue to the rendering of the electrode glyph. Therefore, we determine the depth d_v of each vertex $v \in V$ in view space. A normalization of all d_v to the depth range $[d_{\min}, d_{\max}]$ yields a normalized scalar depth

$$\delta_v = \frac{d_v - d_{\min}}{d_{\max} - d_{\min}} \in [0,1]. \quad (9)$$

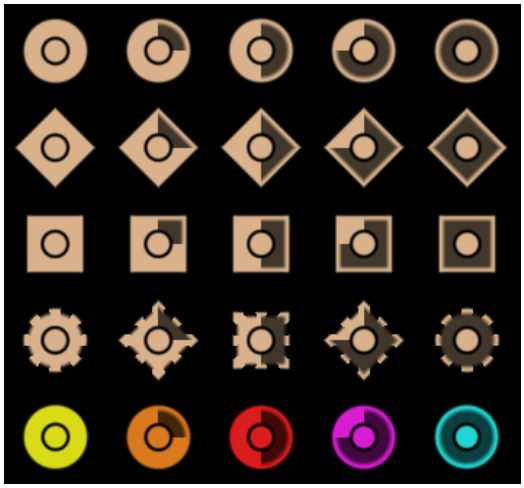

Figure 6: **Different forms of the electrode glyph.** *Columns*: Increasing number of electrical discharges from left to right. *Rows 1-3*: Different shapes used for marking nominal annotations such as abnormalities. *Row 4*: Stipple border binary annotation for different shapes. *Last row*: Color annotation of individual electrodes.

Using this value, we linearly reduce the luminance in HSL space by $l_v = l_0 \cdot (1 - 0.4 \cdot \delta_v)$. This subtle effect significantly improves the depth perception of the rendered electrodes and allows the viewer to infer their spatial ordering.

2.4. Brushing and Linking Concepts

Since we designed our schematic view as a navigation tool for the complex multi-modal 3D data, brushing and linking concepts are an essential part. They allow to the user to interact with the schematic view in terms of selections and annotations, as well as to use it to define the view in one of the linked 2D and 3D visualizations. This allows the clinician to quickly analyze the given data sets, to assess the multi-modal data and to save his findings in the schematic map. To illustrate the usefulness of our visualization in this regard, we present three different interaction methods: First, selection metaphors aid the user in highlighting and selecting certain electrodes of interest and adding annotations. Furthermore, the selected electrodes can be used to automatically fit an MPR plane through the corresponding anatomy for a detailed analysis of the anatomy. Finally, we implemented methods for interactive selection and filtering of DTI fiber tracts.

For the remainder of this section, we assume to have three linked views (cf. Figure 1): Apart from our electrode scheme visualization, we have a multi-modal 2D MPR view, as well as a 3D visualization (e.g. direct volume rendering with integrated geometry) of all available data. However, the pro-

posed methods can certainly be extended with additional views.

2.4.1. Electrode Selection

For easy interaction with the data, the user needs an intuitive and fast method for selecting certain electrodes. Besides a simple single click selection metaphor that toggles the selection state of the clicked electrode, we implemented the selection of multiple electrodes based on the Lasso metaphor. To select multiple electrodes at once, the user draws a freehand polygon enclosing the electrodes into any of the three views (cf. Figure 4). Once the lasso definition is finished, we use the projection matrix of the corresponding view to perform a point-in-polygon test in 2D for each projected electrode. To effectively support non-convex and self-intersecting polygons, we use a variant of the winding number test as described in [Wei94].

For interactive feedback, we use a consistent highlighting scheme for the electrodes linked across all views. Using different variations of a glow effect, we can depict the current selection state, as well as provide an interactive hover feedback for the electrode below the current mouse position (cf. Figures 1 and 4). The glow effect is implemented as an overlay so that it can be shown in any linked view without altering the appearance of the highlighted object itself. It further has the benefit of providing a visual outline even if the electrode is occluded in the current view and thus provides optimal feedback to the user.

2.4.2. Cutting Plane Definition

One essential part of our reference workflow is to correlate the EEG of an electrode with the surrounding anatomy. Though 3D visualizations offer an excellent overview, this task is usually performed with 2D MPRs since they are free of occlusion and allow for an easier and better reading of the actual data. However, manipulating the 2D plane until it shows the region of interest is a time consuming and tedious task. To facilitate this process, the plane can be automatically defined to fit the selected electrodes for which we perform a least squares fitting minimizing the distances of the electrodes to the plane. Since a fully arbitrary orientation may be confusing to the user, the computed fitting can be constrained to be orthogonal to one of the three main axes.

2.4.3. Interaction with DTI Tractography

To demonstrate how our schematic view can be used to interact with geometry, we implemented an interactive filtering of DTI tractography data. This functional modality offers detailed insight into the brain white matter micro structure and global connectivity within the brain. However, the sheer amount and complexity of the data leads to occlusion and visual clutter making it hard to actually extract any kind of information. Therefore, our community developed a wide range of effective filtering methods usually based on a given region of interest [PB13]. With our schematic view, the user can automatically define regions of interest for the planning procedure based on the electrode selection. Given a certain threshold d, we only display fibers whose distance to one of the selected electrode centroid positions is below d (cf. Figure 7).

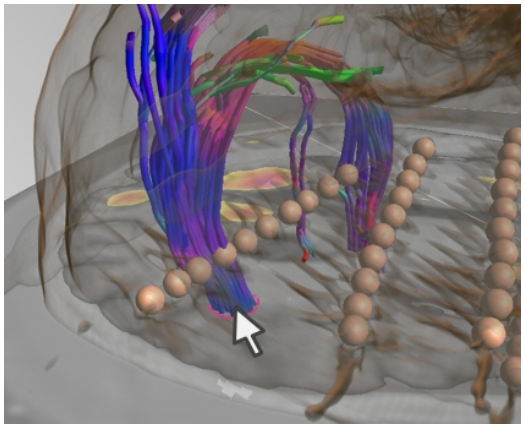

Figure 7: **Interaction with DTI tractography.** Fibers can be filtered based on electrode vincinity or custom regions of interest.

3. Implementation

We integrated the presented methods into the CAMPVis software framework for medical visualization [SGMN14]. Apart from the initial segmentation (cf. Section 2.1) and the force-directed graph layouting (cf. Section 2.2.1) the entire pipeline was implemented on the GPU using OpenGL 4.3 to ensure real-time performance.

Though running entirely on the CPU, our ITK-based [ISNC03] implementation of the segmentation pipeline computes and filters the electrode centroids in less than 0.5 seconds. The graph layouting is also performed on the CPU performing roughly 1000 iterations per second for a graph of 55 vertices. For most projections the graph layouting reaches its minimal energy configuration in less than 1000 iterations. However, in some cases, more iterations are needed so that we set the maximum iteration count to 3000. The layouting is initiated each time the projection of the schematic view has changed and performed in a background thread regularly updating the visualization in order to ensure interactiveness. Due to the rather moderate graph size for our application, a complex GPU implementation would not yield a significant speedup.

By storing the electrode configuration (positions, electrode selection states, annotations, etc.) in Shader Storage Buffer Objects [BDR*12], which allow for easy and flexible data synchronization between CPU and GPU, we can implement the entire rest of our visualization pipeline on the

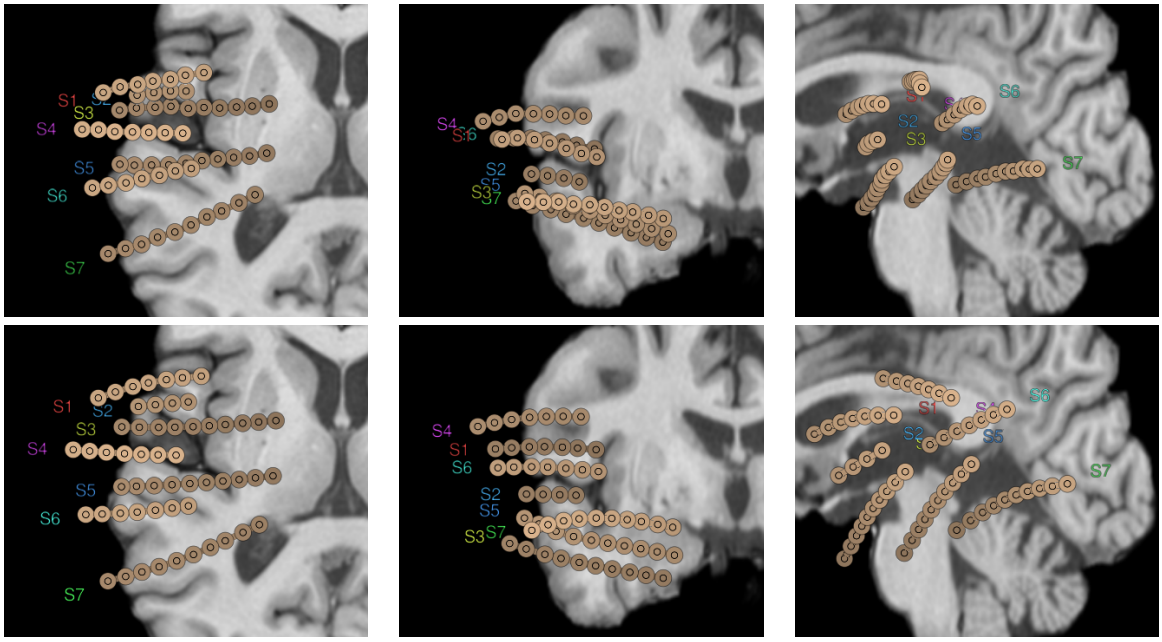

Figure 8: Effect of the **graph layouting for different projections**. The *top row* shows the initial placement of the electrodes for the three main views. The *bottom row* shows the layouted schematic view.

GPU. The rendering of the schematic view is performed in two passes almost entirely using fragment shaders. In the first pass, the reference anatomy image (cf. Section 2.3.2) is rendered as a full screen quad textured from the 3D MRI volume using the current projection. The second pass renders the aligned electrodes on top of the reference image using line and point primitives. To create the electrode glyphs, we exploit `GL_POINT_SPRITE` to customize the rasterized shape in the frament shader. Also, we were able to implement many brushing techniques on the GPU, such as the DTI fiber filtering making use of OpenGL Compute Shaders [SBK*12].

4. Results

For evaluation we use a reference patient data set consisting of 7 depth electrodes with a total of 55 electrode contacts. Figure 1 shows an example of the schematic electrode map during the planning workflow together with a linked 2D MPR view and a 3D direct volume rendering of the data. The overview over the electrode configuration combined with the flexible per-electrode annotations and intuitive brushing and linking techniques facilitates the planning workflow for the clinician.

For evaluation of the graph layouting quality, we developed a custom set of quality measures inspired by [HvKKR14] but adapted to our application and motivated by the original design goals as discussed in Section 2.2:

- **Mean squared vertex displacement** $\widehat{d}$: The mean squared distance a vertex is displaced, defined as

$$\widehat{d} = \frac{1}{|V|} \sum_{v \in V} |p_v^* - p_v|^2, \tag{10}$$

  allowing to quantify the *accuracy* criterion.
- **Number of crossings in the graph** n_c: Since crossing edges increase the visual complexity of the visualization, this serves as a marker for the *intuitiveness* criterion.
- **Average free area** $\widehat{A}_f$: The measure of the average area of the free circle around each vertex

$$\widehat{A}_f = \frac{1}{|V|} \sum_{v \in V} 2\pi * r_{min}(v)^2, \tag{11}$$

  where $r_{min}(v)$ is the distance to the nearest vertex, quantifying the amount of *occlusion* within the final layout.
- **Straightness Error** $E_{\|}$: Quantification of the deviation from a straight line, computed as the squared distance of each vertex from a line fitted to the vertices of the same depth electrode

$$E_{\|} = \sum_{v \in V} (d(v, l_e))^2, \tag{12}$$

  where e is the depth electrode containing a vertex v and l_e is the line fitted to depth electrode e. This is another marker for *intuitiveness* of the layout, since depth electrodes are of mostly straight shape, which should be re-

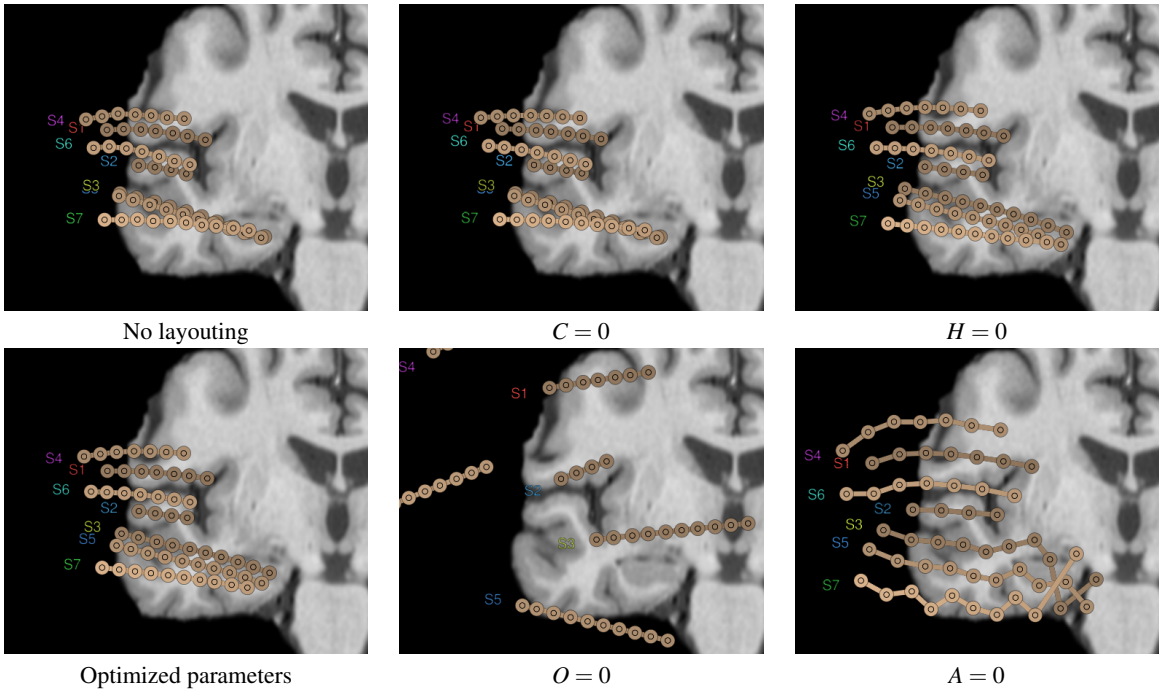

Figure 9: **Influence of the graph layouting forces**. The images in the *left column* show the initial placement of the electrodes and the final layout. The *center and right* columns show the effect on layouting quality if one of the forces is removed.

flected in order to align the view with the user's mental model.

With our current implementation the selection of the four weighting factors C, H, O, and A, controlling the magnitude of the corresponding forces during the graph layouting, also depends on technical constraints, such as the screen resolution, glyph size and visual preferences of the user. Thus, in order to generate the images throughout this manuscript, a fixed set of parameters has been used that was calibrated to the above reference data set.

We performed a parameter evaluation to assess the dependency of the weighting factors on each other and the layouting result. Therefore, we compared a set of original projections without any layouting to the corresponding graph-layouted schematic views. Figure 8 shows how our method succeeds in resolving the occlusions. Furthermore, Figure 9 depicts for the coronal view how the individual forces contribute to the final graph layout. Tables 1 and 2 show the corresponding quantitative results of the introduced quality metrics. The main force to reduce the occlusion is the Coulomb force pushing the vertices apart, thus increasing the free area between vertices. The homing force acts as a counter-force to keep $\widehat{d}$ low and thereby control the accuracy of the layout. The spring forces and the angular forces serve to keep the original shape of the depth electrodes and support the intuitiveness of the resulting layout by minimizing the number of crossings and the straightening the graph.

Table 1: Graph quality metrics for the images shown in Figure 8.

View	before			after			
	n_c	$\widehat{A}_f$	$E_{\|\|}$	n_c	$\widehat{A}_f$	$E_{\|\|}$	$\widehat{d}$
axial	0	973	85	0	1188	94	142
coronal	6	454	143	2	1057	321	261
sagittal	0	155	126	0	719	305	513

Table 2: Influence of the individual weighting factors, quantitative results of the layouts shown in Figure 9.

	n_c	$\widehat{A}_f$	$E_{\|\|}$	$\widehat{d}$
No layouting	4	745	162	0
$C = 0$	4	728	49	0.83
$H = 0$	0	1503	152	109
$O = 0$	0	1543	1.2	22605
$A = 0$	8	4036	11952	1788
Optimized	0	1338	83	84

5. Conclusion

In this work, we presented a novel schematic map of depth electrode configurations in neuro data sets to be used during

neuro resection planning. Using a force-directed graph layouting approach, our schematic view resolves occlusions of electrodes while preserving their original topology to provide the user with an intuitive overview from arbitrary projections. We further propose the electrode glyph to represent single electrodes in our schematic views. It supports different scalar, nominal and binary annotations in order to facilitate the planning workflow for the clinician. Finally, brushing and linking techniques allow for an easy mapping of the electrode EEG data to the corresponding anatomy. This makes our schematic electrode map a powerful tool for navigation in such complex multi-modal data sets.

So far, we see the manual selection of the force weights as the main limitation of our methods. Therefore, as future work, we would like to automatize this process or at least reduce the number of parameters. Furthermore, it would be interesting to explore how our approach can be transferred to other similar clinical applications.

Acknowledgements

We thank Dr. Christian Vollmar from the epilepsy center of the LMU Klinikum München for his help and for providing us with data as well as valuable insight about the clinical application and workflow.

References

[ANC*15] ARNULFO G., NARIZZANO M., CARDINALE F., FATO M., PALVA J.: Automatic segmentation of deep intracerebral electrodes in computed tomography scans. *BMC Bioinformatics 16*, 1 (2015). 5

[BDR*12] BOLZ J., DANIELL P., RICCIO C., SELLERS G., MERRY B., KESSENICH J.: ARB Extension #137: ARB_shader_storage_buffer_object. 9

[BG15] BC J., GD C.: Resective epilepsy surgery for drug-resistant focal epilepsy: A review. *JAMA 313*, 3 (2015), 285–293. 4

[BHWB07] BEYER J., HADWIGER M., WOLFSBERGER S., BUHLER K.: High-quality multimodal volume rendering for preoperative planning of neurosurgical interventions. *Visualization and Computer Graphics, IEEE Transactions on 13*, 6 (Nov 2007), 1696–1703. 5

[BLE*13] BOCK A., LANG N., EVANGELISTA G., LEHRKE R., ROPINSKI T.: Guiding deep brain stimulation interventions by fusing multimodal uncertainty regions. In *Visualization Symposium (PacificVis), 2013 IEEE Pacific* (Feb 2013), pp. 97–104. 5

[BRS*04] BOESEN K., REHM K., SCHAPER K., STOLTZNER S., WOODS R., LÜDERS E., ROTTENBERG D.: Quantitative comparison of four brain extraction algorithms. *NeuroImage 22*, 3 (2004), 1255 – 1261. 5

[DB99] DI BATTISTA G.: *Graph Drawing: Algorithms for the Visualization of Graphs*. An Alan R. Apt Book. Prentice Hall, 1999. 5

[DPL*11] DIEPENBROCK S., PRASSNI J.-S., LINDEMANN F., BOTHE H.-W., ROPINSKI T.: Interactive Visualization Techniques for Neurosurgery Planning. BÃijhler K., Vilanova A., (Eds.), Eurographics Association, pp. 13–16. 5

[FR91] FRUCHTERMAN T. M. J., REINGOLD E. M.: Graph drawing by force-directed placement. *Software: Practice and Experience 21*, 11 (1991), 1129–1164. 5, 7

[HvKKR14] HOFFMANN M., VAN KREVELD M., KUSTERS V., ROTE G.: Quality ratios of measures for graph drawing styles. In *Canadian Conference on Computational Geometry, CCCG* (2014). 10

[ISNC03] IBANEZ L., SCHROEDER W., NG L., CATES J.: *The ITK Software Guide*, first ed. Kitware, Inc., 2003. ISBN 1-930934-10-6. 9

[KF03] KURUVILLA A., FLINK R.: Intraoperative electrocorticography in epilepsy surgery: useful or not? *Seizure 12*, 8 (2003), 577 – 584. 4

[PB13] PREIM B., BOTHA C.: *Visual Computing for Medicine: Theory, Algorithms, and Applications*. The Morgan Kaufmann Series in Computer Graphics. Elsevier Science, 2013. 4, 5, 9

[PJ54] PENFIELD W., JASPER H.: Electrocorticography. *Epilepsy and the Functional Anatomy of the Human Brain* (1954), 692–738. 4

[RRRP08] RIEDER C., RITTER F., RASPE M., PEITGEN H.-O.: Interactive visualization of multimodal volume data for neurosurgical tumor treatment. *Computer Graphics Forum 27*, 3 (2008), 1055–1062. 5

[SBK*12] SELLERS G., BROWN P., KOCH D., KESSENICH J., MEMBERS OF THE ARB WORKING GROUP: ARB Extension #122: ARB_compute_shader. 10

[SDB*04] SÏ£¡GONNE F., DALE A., BUSA E., GLESSNER M., SALAT D., HAHN H., FISCHL B.: A hybrid approach to the skull stripping problem in {MRI}. *NeuroImage 22*, 3 (2004), 1060 – 1075. 5

[SGMN14] SCHULTE ZU BERGE C., GRUNAU A., MAHMUD H., NAVAB N.: *CAMPVis – A Game Engine-inspired Research Framework for Medical Imaging and Visualization*. Tech. rep., Technische Universität München, 2014. 9

[Sil12] SILVERSTEIN J.: Mapping the motor and sensory cortices: A historical look and a current case study in sensorimotor localization and direct cortical motor stimulation. *The Neurodiagnostic Journal 52*, 1 (2012), 54–68. 4

[Sug02] SUGIYAMA K.: *Graph Drawing and Applications for Software and Knowledge Engineers*. Series on software engineering and knowledge engineering. World Scientific, 2002. 5

[TAATF*14] TAIMOURI V., AKHONDI-ASL A., TOMAS-FERNANDEZ X., PETERS J., PRABHU S., PODURI A., TAKEOKA M., LODDENKEMPER T., BERGIN A., HARINI C., MADSEN J., WARFIELD S.: Electrode localization for planning surgical resection of the epileptogenic zone in pediatric epilepsy. *International Journal of Computer Assisted Radiology and Surgery 9*, 1 (2014), 91–105. 5

[Wei94] WEILER K.: An incremental angle point in polygon test. *Graphics gems IV 4* (1994), 16. 9